Observed low frequency variability of the Brazil Current front

Gustavo Jorge Goni,[1] Francis Bringas,[1,2] and Pedro Nicolas DiNezio[1,2]

Received 4 April 2011; revised 28 June 2011; accepted 18 July 2011; published 29 October 2011.

[1] The Brazil Current is a weak western boundary current, the southwest component of the South Atlantic subtropical gyre, which is the main conduit of upper ocean waters in the region. The objective of this work is to report on observed low frequency variability of the Brazil Current front using satellite-derived sea height anomaly and sea surface temperature observations during the 1993–2008 period. The variability of the front is studied in terms of the separation of the Brazil Current front from the continental shelf break. During the study period, estimates of this parameter vary 6 degrees in latitude, and the mean monthly estimates exhibit a shift to the south of approximately 1.5 degrees. Statistically significant changes are not observed in the geostrophic transport of the Brazil and Malvinas currents, suggesting that the low-frequency changes of the Brazil Current front are governed by different mechanisms than the seasonal variability of these surface currents. Surface drifter trajectories and simulations using synthetic drifters are consistent with the observed shift to the south of the Brazil Current front. Trends of eddy kinetic energy, sea height anomaly, sea surface temperature and wind stress curl are also in agreement with the variability reported here. Wavelet transform analysis revealed interesting changes in the periodicity of the latitude of separation of the Brazil Current front from the continental shelf break, with periods ranging from semiannual to biannual. Longer records, together with comprehensive numerical experiments, will ultimately be needed to determine the origin of these changes.

Citation: Goni, G. J., F. Bringas, and P. N. DiNezio (2011), Observed low frequency variability of the Brazil Current front, *J. Geophys. Res.*, *116*, C10037, doi:10.1029/2011JC007198.

1. Introduction

[2] The subtropical gyre is the dominant large-scale feature of the South Atlantic Ocean. This large-scale circulation comprises several components. The southern branch of the South Equatorial Current is the northern limb of the gyre, which bifurcates off Brazil at approximately 15°S, resulting in the formation of the southward flowing Brazil Current (BC), the western boundary current of the gyre. The eastward flowing South Atlantic Current and the northward flowing Benguela current complete the circulation, delimiting the southern and eastern boundaries of the subtropical gyre, respectively [*Peterson and Stramma*, 1991]. The dynamics in the southwestern Atlantic are dominated by the convergence of the Malvinas Current (MC), which is northward flowing and cold, with the Brazil Current, the southward flowing warm weak (5 to 22 Sv; 1 Sv = 10^6 m^3s^{-1}) [*Peterson and Stramma*, 1991] western boundary current (Figure 1) in this region. The area of convergence of these two currents, called the Brazil-Malvinas Confluence [*Gordon and Greengrove*, 1986], exhibits complex frontal motions and patterns with the simultaneous presence of warm and cold rings and eddies. Observations indicate that the latitude of the Confluence changes seasonally [*Matano*, 1993] and has large year-to-year variability [*Goni and Wainer*, 2001]. A detailed study of the Brazil Current frontal variability in the Confluence region using very high resolution (4 km) sea surface temperature (SST) observations during a 9-year time span [*Saraceno et al.*, 2004] reported average values of SST gradients of 0.3°C/km, and the existence of several types of fronts as determined by their thermal and/or dynamic structure and depth.

[3] The variability in the transport of the MC has also been studied using altimetry observations combined with current meter data [*Vivier and Provost*, 1999b]. This study showed that the time series of volume transport exhibits dominant periods of 50–80 days and close to 180 days, with large interannual variability. Most recently, it has been reported that the transport of this current varies widely between 10 and 88 Sv [*Garzoli*, 1993; *Peterson*, 1992] and that it recently experienced a change to a seasonal cycle [*Spadone and Provost*, 2009], probably due to remote wind-forcing. However, little energy was found at the annual period, suggesting that the MC has only a small influence on the annual migration of the Confluence. Most of the variability in the South Atlantic Ocean is concentrated in the region of Confluence and in the Agulhas retroflection, where the RMS of sea height and eddy kinetic energy exhibit values reaching

[1]NOAA Atlantic Oceanographic and Meteorological Laboratory, Miami, Florida, USA.
[2]Cooperative Institute for Marine and Atmospheric Studies, University of Miami, Miami, Florida, USA.

Copyright 2011 by the American Geophysical Union.
0148-0227/11/2011JC007198

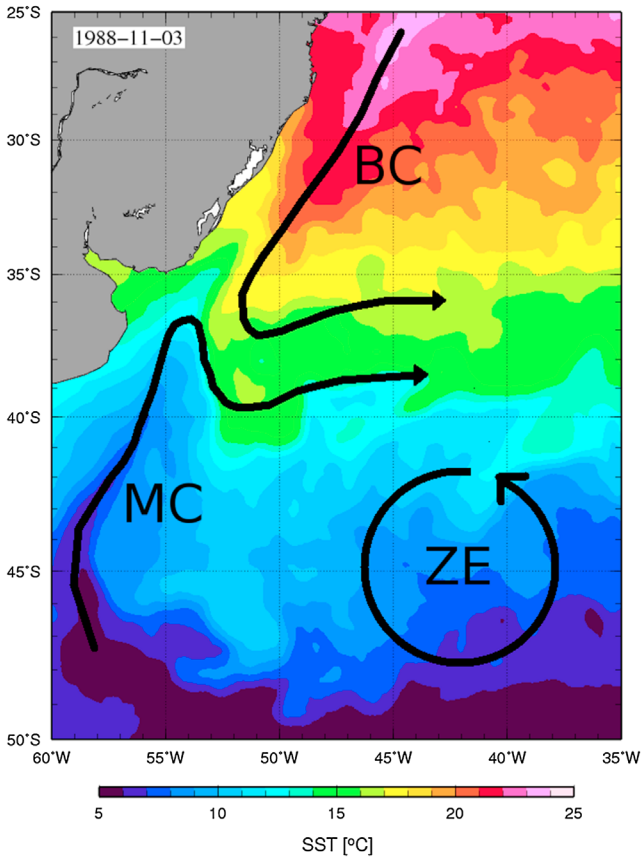

Figure 1. Sea surface temperature (SST) composite for 11 November 1988 exhibiting a southern incursion of the southward flowing warm Brazil Current. The region of convergence between the Brazil Current (BC) and the cold northward flowing Malvinas Current (MC) is called the Confluence region. The semi-permanent anticyclonic feature centered at approximately 45W is known as the Zapiola Eddy (ZE).

25 cm and 103 cm^{-2} s^{-2}, respectively (Figure 2). Lower values of sea surface height variability are found in the center of the subtropical gyre, between 20°S and 40°S.

[4] The objective of this work is to report observed low frequency variability in the Brazil Current front (BCF) and explore its link with observed changes in the wind field. The insufficient hydrographic observations available in the South Atlantic render satellite altimeters and radiometers as the only observing platforms capable to investigate long-term thermal and dynamical changes in the region. The 15-year-long altimetry record allows analyzing the surface height and subsurface trends that may correspond to several types of changes, including year-to-year, decadal signals, and secular changes. In order to report these results, this manuscript is organized as follows. The data used in this work are presented in section 2. In section 3, the variability of the BCF is analyzed in terms of the separation of the BC from the continental shelf break using SST and sea height anomaly (SHA) fields, as well as synthetic Lagrangian drifters. The low-frequency variability of the BCF is then compared with long-term changes of geostrophic transport of the BC and MC, and of the local wind field. Section 4 presents the summary and conclusions.

2. Data

[5] The temporal and spatial resolution of the sustained in situ oceanographic observations in the southwestern Atlantic Ocean are not sufficient to resolve mesoscale features. Only satellite derived observations of SHA, SST, and reanalysis winds offer the sufficient temporal and spatial resolution to study the low-frequency variability of large and mesoscale oceanographic structures, such as the subtropical gyre and the BCF. Over the subtropical oceans, adjacent altimeter ground tracks are between 100 km and 250 km apart, which are considerably larger than the internal Rossby radius of deformation (40 km), making observations from a single satellite altimeter unable to resolve the mesoscale field. For this reason, the resolution capability of satellite-derived SHA fields for mesoscale studies has been a matter of rigorous study [e.g., *Le Traon et al.*, 1995; *Greenslade et al.*, 1997]. Studies have reported that the resolution of ocean mesoscale processes is improved by combining observations from at least two satellites to resolve mesoscale features in midlatitude regions [*Le Traon and Ogor*, 1998; *Le Traon and Dibarboure*, 1999].

[6] The SHA fields used here are produced by AVISO, with weekly resolution on a 1/4° latitude × 1/4° longitude grid by combining observations of the Jason1, TOPEX/Poseidon, ENVISAT, GFO, ERS1 and 2, and GEOSAT altimeters [*Le Traon et al.*, 1998; *Ducet et al.*, 2000]. These fields are anomalies with respect to the mean of the 1993–1999 period. The altimetric observations used to produce these gridded fields were obtained from two to four satellites throughout the period January 1993 to December 2008. The satellite coverage guarantees that these gridded SHA fields resolve variability of the ocean surface associated with dynamical and thermal fronts, current meandering, and their associated rings. The altimeter data set is used in two ways in this work: a) to investigate the position of the BCF as determined by the location of the jet of the BC; and b) to analyze the trajectory of synthetic drifters deployed in geostrophic velocity fields estimated from altimetry observations.

[7] In the South Atlantic, four main modes of low frequency sea surface height variability have been identified using altimetry observations: 1) the subtropical basin-scale mode corresponding to zonal shifts in the subtropical gyre that explains more than half of the sea level variance; 2) the tropical mode located in the northern portion of the basin; 3) a 2–3 year mode in the Confluence region corresponding to meridional variations of the latitude of the confluence and to variations in the regional distribution of eddy variability; and 4) the Cape Basin mode east of South Africa [*Witter and Gordon*, 1999; *Fetter and Matano*, 2010]. Furthermore, long-term changes in the SHA fields also provide information on the low frequency variability of the global upper ocean circulation and have been extensively used to monitor trends in sea level [e.g., *Cabanes et al.*, 2001]. In the southwestern Atlantic, the SHA fields are characterized mainly by an alternation of areas of low and high values related to the motion of the Brazil and Malvinas currents and their associated fronts and meandering, and with the shedding of mesoscale rings [*Goni and Wainer*, 2001].

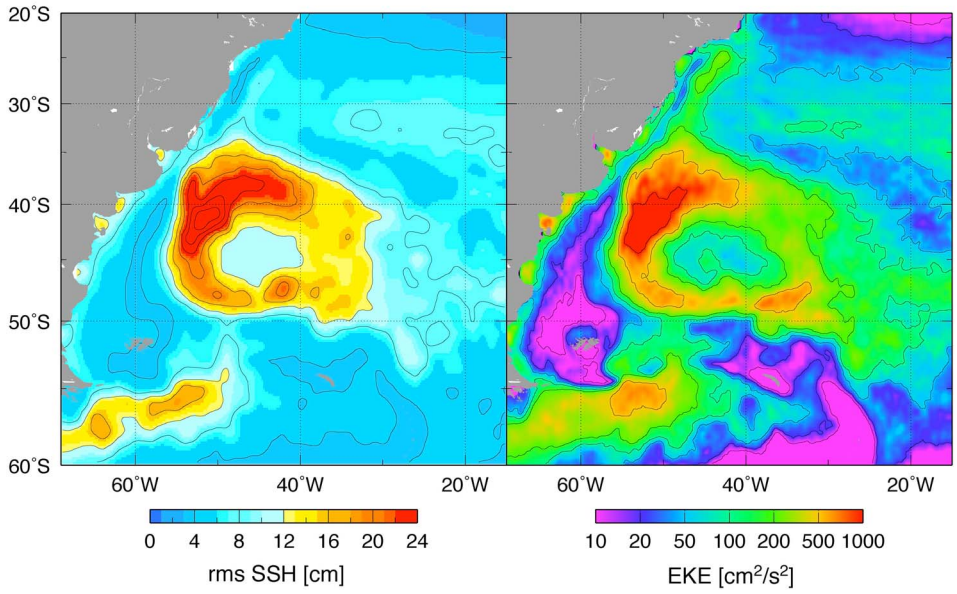

Figure 2. Satellite altimetry-derived RMS of sea surface height (SSH) and eddy kinetic energy (EKE) in the South Atlantic Ocean during the period 1993–1999.

[8] High-resolution satellite-derived SST observations are also used to study the low frequency variability of the BCF. Microwave Optimally Interpolated SST fields obtained from observations retrieved by the TMI and AMSR-E radiometers onboard the TRMM and Aqua satellites, respectively, are used for the period 1998 to 2006. These fields have a daily resolution on a 0.25 degree grid. The data set is completed with gridded fields obtained using SST observations from the Advanced Very High Resolution Radiometer (AVHRR). These fields are produced with a resolution of 2 days on an 18 km equal-area grid for the period 1993 to 1997 [*Ryan et al.*, 1996]. The spatial and temporal resolutions of these fields also have the capability to resolve the strong mesoscale variability in the Confluence required to detect long-term changes without aliasing.

[9] Monthly mean surface wind stress fields from the NCEP/NCAR reanalysis project [*Kalnay et al.*, 1996] are used to explore the role of wind-forcing in the long term changes of the BCF and the South Atlantic subtropical gyre. The zonal (τ^x) and meridional (τ^y) components of the surface momentum flux are available on a T62 Gaussian grid (approximately 2 × 2 degree resolution) from which the surface wind stress (τ) is computed. Additionally, trajectories of satellite tracked drogued drifters in the South Atlantic during 1992–2007 are used to support some of the results obtained from the satellite-based methodologies.

3. The Brazil Current Front

3.1. Separation of the Front From the Continental Shelf Break

[10] The variability of the BCF is examined in terms of the separation of the BC from the continental shelf break, i.e., the intersection of the BCF with the continental shelf break computed using sea surface height (SSH) fields from altimetry and satellite-derived fields of SST (Figure 3). This separation point is defined as the location of the maximum SSH and SST gradient along the 1000 m isobath. The SSH fields are derived from the SHA gridded values described in Section 2, adding the dynamic height climatology referenced to 750 m [*Conkright et al.*, 1998]. In both cases, the values of the gradient of SSH and SST along the 1000 m isobath are smoothed using a 10th order Butterworth filter with a cutoff wavelength of 500 km. This cutoff wavelength allows for the removal of spatial gradients associated with eddies, while preserving only the SSH and SST gradients associated with the BCF. The location of the maximum gradient is then identified in this smoother function.

[11] Frontal locations determined from SST and SSH fields may not always agree, possibly because they represent surface and subsurface frontal positions, respectively. The separation of the BCF from the shelf break shows strong year-to-year variability with annual amplitudes that range from 1° to almost 6°, consistent with previously reported results [*Goni and Wainer*, 2001]. Monthly mean values of the separation indicate that the southernmost (northernmost) positions occur in JFM (ASO). The annual and semiannual components dominate the variability of the separation. However, the southernmost location of the BCF, which is dominated by higher frequency variability associated with mesoscale features, has been reported not to exhibit a clear annual periodicity as the frontal separation [*Lentini et al.*, 2006].

[12] The time series of monthly values of the separation derived from SSH and SST fields indicate that in the mean the frontal location derived from satellite altimetry (jet of the current) is consistently farther to the north than the one derived from SST (maximum SST horizontal gradient) by approximately 0.4° (Figure 4). The monthly anomalies of the separation indicate that in the mean their locations have shifted to the south during the study period (Figures 5a and 5b). Results indicate that during 1993–1997 the separation

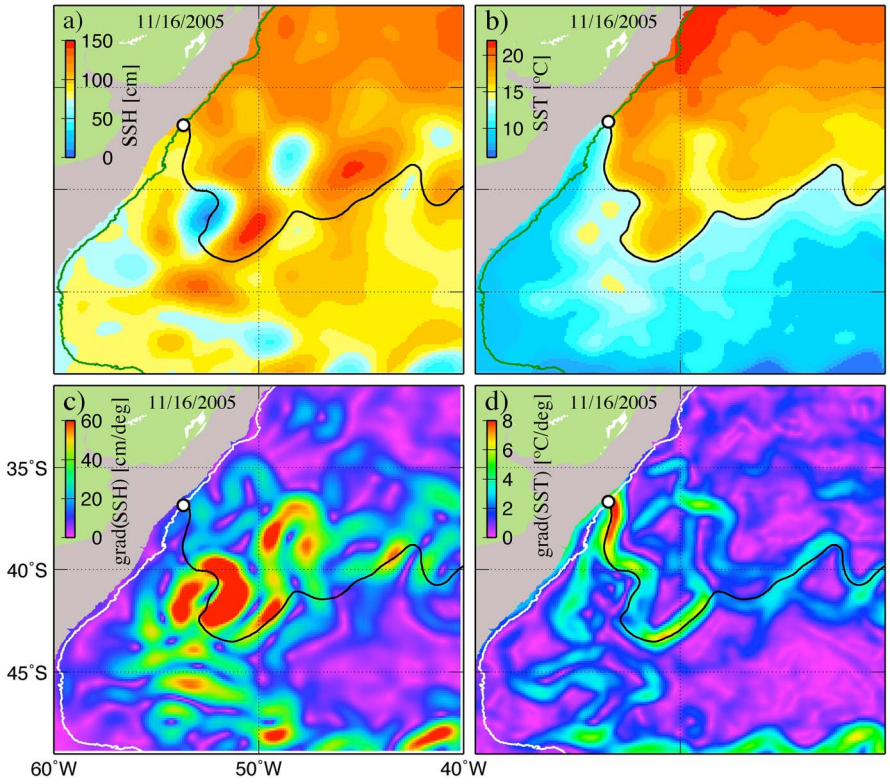

Figure 3. (top) Fields of (left) sea surface height (SSH) and (right) sea surface temperature (SST) corresponding to November 16, 2005. (bottom) The horizontal gradients of the fields above. The continental shelf break, the location of the front as determined from the sea surface temperature field, and (white circle) the separation of the front from the continental shelf break (1000 m isobath) are shown.

of the BCF was mostly north of its mean location, while during 2004–2008 it was mostly to the south (Figure 5a). The least squares linear trends of the separation derived from altimetry and SST fields are (−0.81 ± 0.38) degree per decade and (−0.39 ± 0.33) degree per decade, respectively. Although the SSH- and SST-derived values are different, they both have the same sign, and the difference may be related to a sampling issue and/or to the fact that the SST is more representative of the sea surface, while the SSH is more representative of the subsurface location of the front.

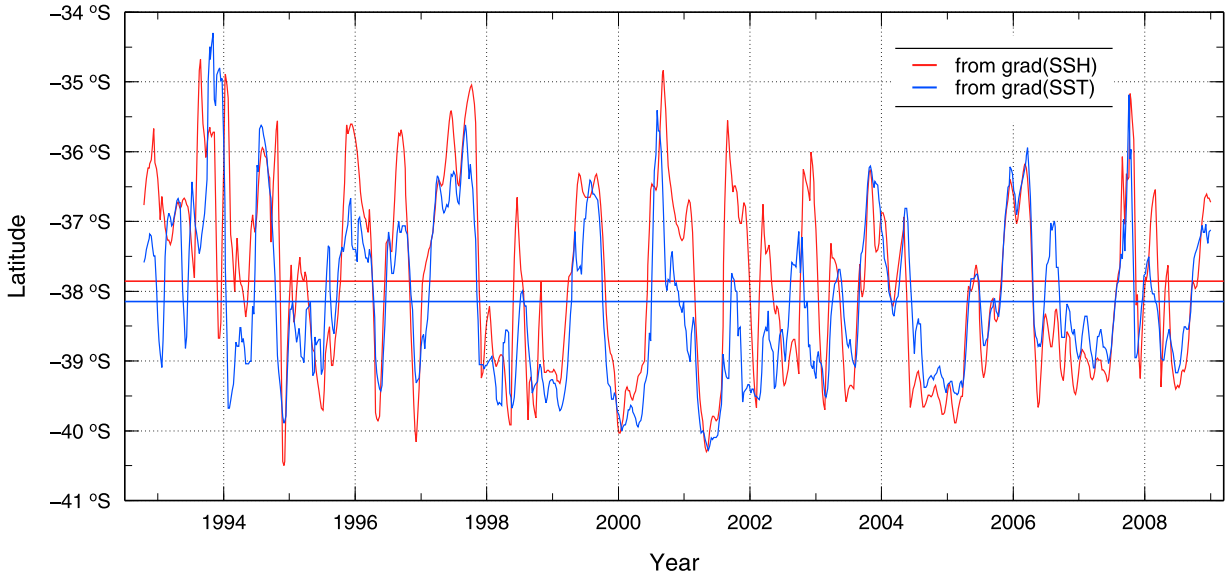

Figure 4. Time series of the separation of the Brazil Current front (BCF) from the continental shelf break (1000 m isobath) computed using (red) sea surface height and (blue) sea surface temperature fields.

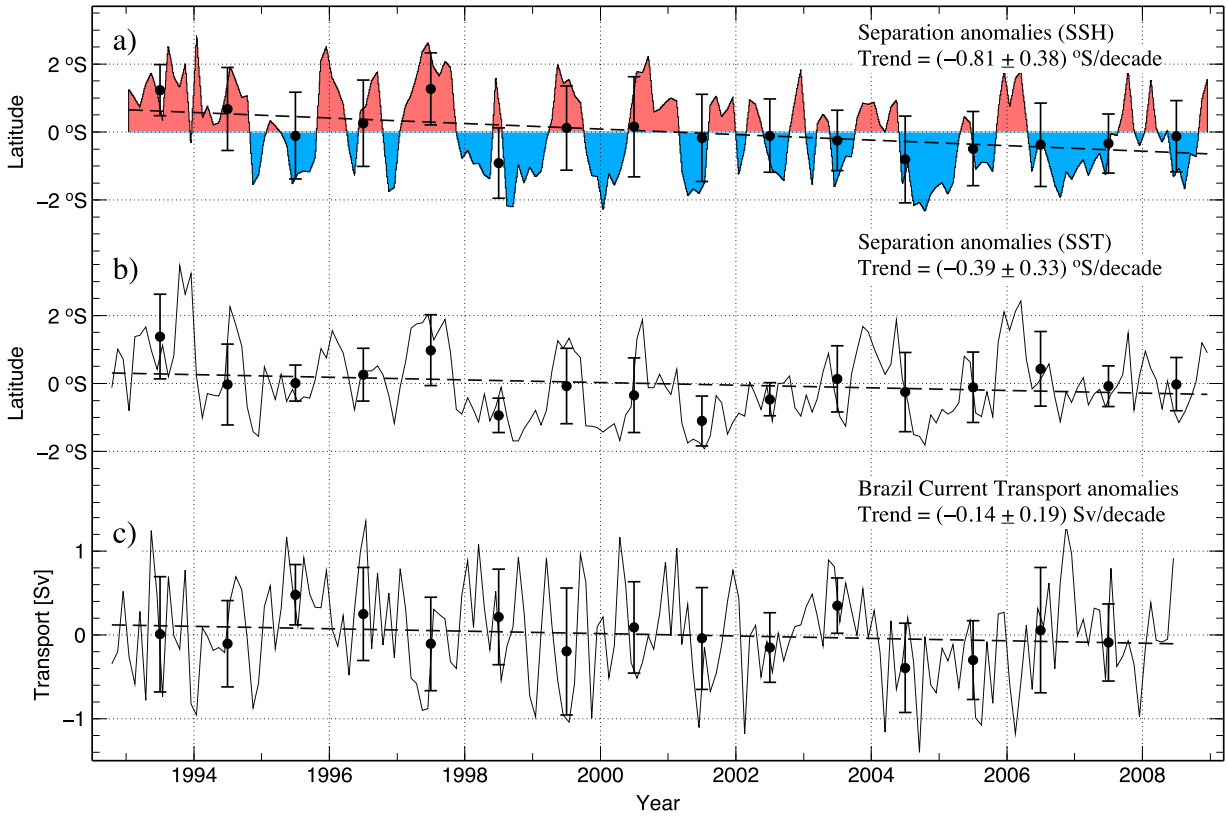

Figure 5. Monthly anomalies of the latitude of separation of the BC from the continental shelf break derived from (a) altimetry and (b) SST. (c) Monthly anomalies of geostrophic transport of the BC. The circles indicate mean annual values with their standard deviation represented by the bars, while the red (blue) color in Figure 5a indicates the positive (negative) anomalies. The dashed lines are the least squares linear fit of the monthly anomalies time series, the value of the slope (trend) is indicated in the figure for each case, including the standard error.

The auto-correlation function of the seasonally removed monthly anomalies indicates an integral time scale of 5 months. Thus, we reduced the degrees of freedom of the time series by a factor of 5 prior to computing the standard error of the linear trend. The uncertainty in the linear trends estimates is given by the standard error computed from the time series with the climatological annual cycle removed, considering only the dispersion of the data points and not their experimental error, as well as the actual number of degrees of freedom. This standard error represents a lower bound for the uncertainty, which would be larger if other sources of errors are considered. These trends are statistically compatible and different from zero within at least one standard error. In addition, these trends may partly be the result of a few large year-to-year variations instead of a linear trend, which cannot be properly assessed because of the short length of the record. The trend to the south is more evident in the separation than in the southernmost location (not shown). The lack of a robust signal in the southernmost location could be the result of intermittent ring shedding, rendering the long-term trend undetectable [*Lentini et al.*, 2006]. Moreover, the total shift during 1993–2006 is larger than 1 degree, a magnitude several times larger than the spatial resolution of the satellite-derived SHA and SST fields, therefore making these results statistically significant. These same qualitative results were not found by *Goni and Wainer* [2001] because their time series extended only until 1998, and the larger changes in frontal motion started that same year. These estimates are consistent with those published [*Lumpkin and Garzoli*, 2011] but differ from them in that the BCF variability is investigated here in terms of the frontal separation from the continental shelf break and not from a line given by an altimeter ground track. In addition, trends obtained in this work are statistically different from zero within one standard error.

[13] Shorter period variability of the BCF is examined using the technique of wavelet transform (WT) [*Grinsted et al.*, 2004]. Unlike traditional spectral analysis, WTs can capture variations in variance with time. A WT of the altimetry-derived separation of the BCF from the continental shelf break (Figure 6) shows the spectral power with times (abscissa) and signal periods (ordinate) indicating periods when the BCF shows the highest variance. The *cone of influence*, limited by the dashed line, corresponds to times and frequencies that are not subject to aliasing due to edge effects. The solid contours correspond to when the spectral power is distinct from the null hypothesis with 67% or greater of confidence. Values inside this cone are not proportional to the variability; but they are a measure of the different frequencies composing the time series at a given time. In this type of analysis the null hypothesis is that the signal is red noise, in this case a univariate lag–1

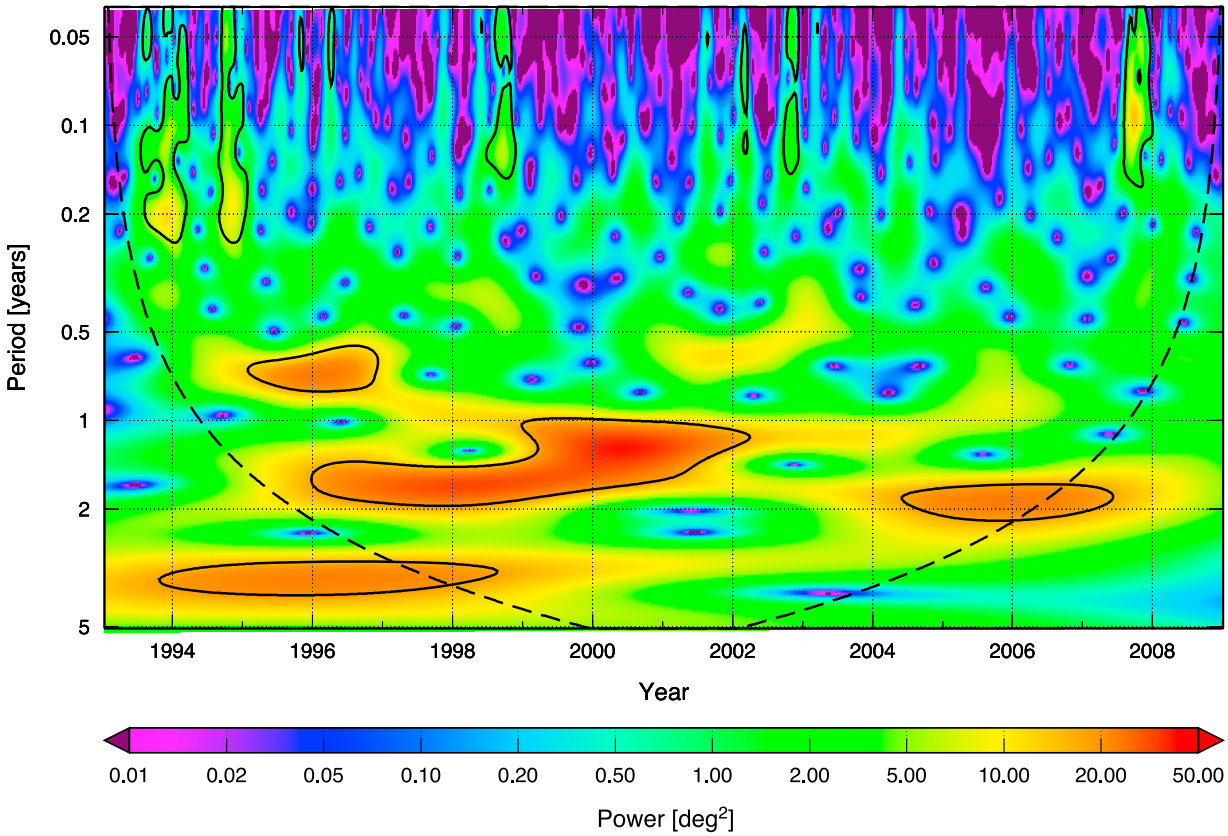

Figure 6. Wavelet Spectrum Density of the sea surface height derived time series of the separation of the Brazil Current front from the continental shelf break. The solid black contour represents the peak-based significance levels, computed at 95%. The dashed curve indicates the cone of influence.

autoregressive process. The WT analysis reveals that the separation of the BCF has strong variability on semiannual to biannual time scales, with the biannual component starting in 2004. This variance is located within the cone of influence, reflecting an actual change in the spectral characteristics of the time series of the separation of the BCF from the continental shelf break. Lower frequency variability is also observed at periods of about four years during the early part of the record, but longer records will be needed to assess the robustness of this result. This lower frequency variability could be responsible for the southward trend detected over the duration of the 16-year record of this study.

3.2. Southern Excursions of the Brazil Current Front

[14] Trajectories of Lagrangian drifters are also analyzed to investigate if the variability observed from the SST and altimetry-derived estimates can be supported with observations derived from an independent platform such as surface drifters. We used the trajectories of all drifters that traveled within a closed box located in the Brazil Current and limited by 52°W-48°W and 34°S-32°S. These drifters were followed after entering this box and their trajectories were separated into two groups, corresponding to the periods 1993–1999 and 2000–2006, and each of them for the months of JFM and JAS. An examination of their trajectories indicates that for the months of JAS during the period 2000–2006 the trajectories are more to the south than during 1993–1999 (Figure 7). However, these results cannot be considered conclusive because there are only 49 drifters that traveled in this region, which represents a very sparse spatial coverage and low temporal resolution.

[15] Alternatively, in order to explore dynamical changes in the confluence region we compute the trajectories of synthetic drifters by integrating the near-surface geostrophic velocities derived from satellite altimetry. The surface currents (u_g, v_g) are computed from geostrophy as:

$$\begin{aligned} u_g &= -g(fa^{-1})\partial\eta/\partial\lambda, \\ v_g &= -g(fa^{-1}\cos\lambda)\partial\eta/\partial\theta \end{aligned}, \qquad (1)$$

where λ is latitude, θ is longitude, g is gravity, f is the Coriolis parameter, a is the Earth radius, and η is the sea height. The time-mean component of the sea height field, η, is obtained from a methodology that combines the geoid, satellite altimetry, and in situ hydrography [*Rio and Hernandez*, 2004]. The time-varying component is the SHA derived from satellite-altimetry observations. Since this velocity field is purely geostrophic, the particle trajectories do not simulate surface drifters, but drifters flowing in the subsurface right below the Ekman layer. The synthetic drifter trajectories are integrated using a fourth order Runge–Kutta method with a fixed 7-day time step and a linear interpolation scheme. Every 4 weeks starting on Jan 1, 1993, 230 drifter particles were released from a 2° × 2° box centered at

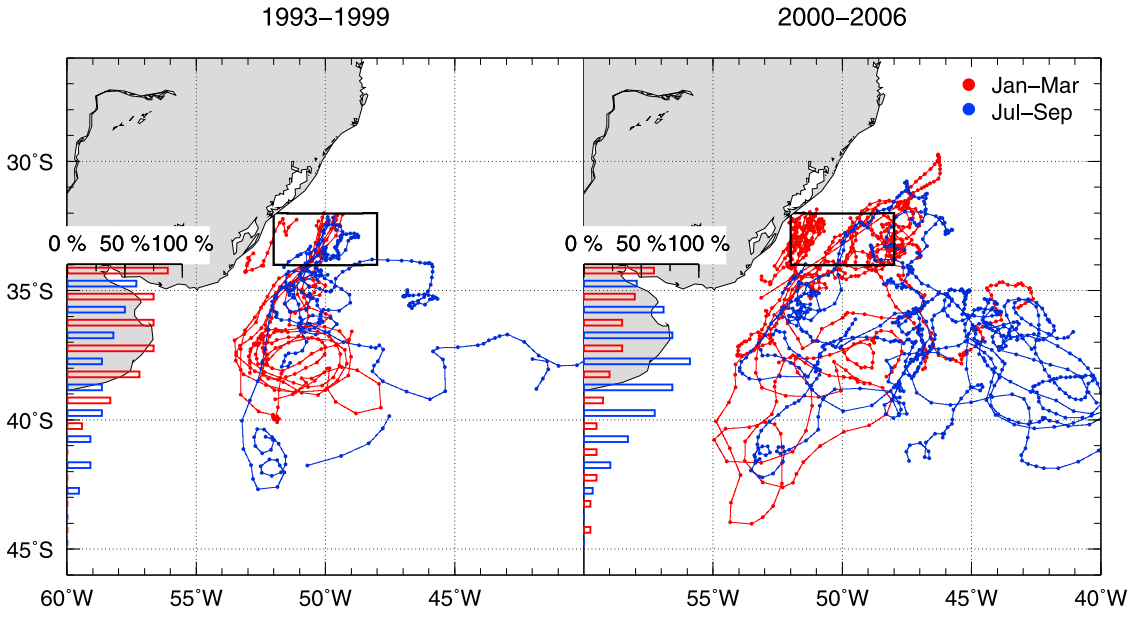

Figure 7. Surface drifter trajectories during (left) 1993–1999 and (right) 2000–2006 during January–March (red) and July–September (blue). Only trajectories for drifters traveling across the box centered at 50°W 33°S are included. The histograms to the left of each panel indicate the percentage of the number of drifters that reach each latitude. For the period 1993–1998 there were 18 drifters and during the period 2000–2006 there were 31 drifters.

50°W, 34.5°S and integrated for 2 years (Figure 8). This box is located off the coast of South America and within the location of the time-mean jet of the Brazil Current and upstream from the Brazil-Malvinas Confluence, guaranteeing that most synthetic drifters will be trapped in the Brazil Current. The particles initially follow the Brazil Current southward into the Confluence region, although a few particles recirculate close to the box and never reach the confluence. The 2-year length of the integration allows some of the particles to follow the large-scale circulation of the South Atlantic subtropical gyre (Figure 8). A few trajectories follow the South Atlantic Current and circulate around the gyre, reaching back to the Brazil Current during the 2-year integration. However, the majority of the trajectories recirculate closer to the confluence. Additionally, the trajectories show variability associated with mesoscale features of the circulation captured by the altimetric observations.

[16] The particle trajectories are used to compute the density of particle locations as the number of drifters that traveled over each 1/4° × 1/4° bin of the domain throughout a year. Each yearly map of particle densities includes drifter trajectories corresponding to 13 releases of particles simulated throughout that year. Over a given year, the spatial distribution of the density of particles captures the large-scale circulation of the South Atlantic subtropical gyre showing values of about 100 particles per 1/4° × 1/4° bin near the center of the gyre and very low values at the boundaries of the gyre (Figure 9, top and middle). The difference in particle densities between years 2006 minus 1993 shows an increase in the number of particles reaching southern locations in the confluence region, therefore providing more evidence for a southward shift of the BCF (Figure 8, bottom).

3.3. Brazil and Malvinas Current Transports

[17] Some theoretical and modeling studies have successfully explained why the separation of the BC from the continental margin is located north of the zero wind stress curl (WSC) contour and is also governed by the relative strength of the MC and the BC [*Veronis*, 1973; *Matano*, 1993]. Following these arguments, changes in the geostrophic transport of the BC and MC are analyzed to investigate a possible link with the observed BCF trend.

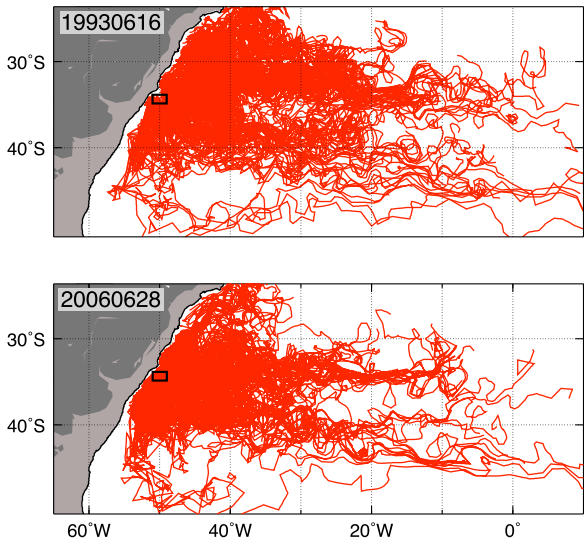

Figure 8. Trajectory of 230 synthetic Lagrangian drifters deployed on (top) June 16, 1993; and (bottom) June 28, 2006. The square corresponds to the box where the drifters were deployed. The light gray region corresponds to continental shelf and the thin black line to the 1000 m isobath.

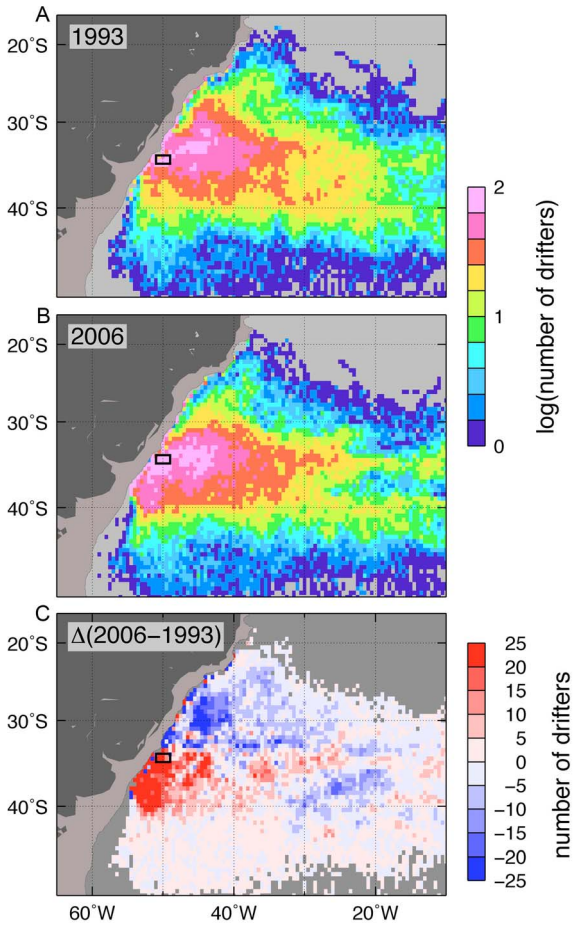

Figure 9. Density of drifter locations, expressed as the number of drifter locations on 1/4deg × 1/4deg boxes, derived from synthetic trajectories of drifters during years (a) 1993 and (b) 2006. Drifter particles are deployed every two months from the box centered at 50°W 34.5°S located off the coast of South America. The color scale is logarithmic to emphasize the strong gradients in drifter density associated with the Brazil Current front. (c) Change in density of drifter locations between years 1993 and 2006.

[18] The BC geostrophic transport across a descending altimeter ground track is estimated using the SHA values added to the mean dynamic height referenced to 1000 m, using the same methodology of *Goni and Wainer* [2001]. The time series of this transport shows strong annual and semiannual variability, with annual mean values that range from 5 to 20 Sv. The annual cycle is less clear in the MC [*Vivier and Provost*, 1999a, 1999b]. Both time series show large interannual variability with year-to-year changes up to 10 Sv consistent with these previous studies. The least squares trend of the time series of the BC transport (Figure 5c) of (−0.14 ± 0.19) Sv per decade is not only negligible, but also statistically compatible with the zero trend at about one standard error. This result indicates no change in the Sverdrup transport of the South Atlantic subtropical gyre, consistent with the spatial patterns of the WSC trends (Figure 10d), which show no large-scale, long-term changes.

[19] Studies have shown that the MC transport has a minor role in the annual and interannual variability of the Confluence region [*Vivier and Provost*, 1999a; *Goni and Wainer*, 2001]. A shift from a semiannual to a seasonal cycle during the year 2000 was reported in the transport of this current [*Spadone and Provost*, 2009], probably due to remote wind-forcing. This longer time series shows a least squares trend of (−0.05 ± 0.11) Sv per decade, which is also compatible with zero trend at about 0.5 standard error. Ultimately, the absence of long-term changes in transport of the BC and MC suggests a different physical mechanism driving the observed southward trend of the BC separation.

3.4. Year-to-Year Trends in the Confluence Region

[20] Least squares linear trends of the time series estimated for each grid point of the SHA, eddy kinetic energy (EKE), SST, and wind stress fields in the South Atlantic are used to analyze the spatial structure of the subtropical gyre changes during 1993–2006. The mean value of the SHA trend is approximately 3.0 cm per decade, with extreme SHA trend values of −6.4 and 21 cm per decade found in the southwest tropical Atlantic (Figure 10a). The SHA trends over the South Atlantic are significant to the 95% level. Sea height changes are mainly due to steric effects and mass changes (e.g., fresh water fluxes). Long-term SHA trends are assumed here to mostly correspond to changes in steric sea level and, therefore, heat storage, as supported by previous research [*Willis et al.*, 2004]. The region between 30°S and 40°S in the southern portion of the subtropical gyre exhibits the largest trends, which are indicative of a change in upper ocean thermal conditions.

[21] The geostrophic EKE is computed from the altimetry fields as $(g^2/2\,f^2)(\eta_x'^2 + \eta_y'^2)$, where g is the acceleration of gravity, f is the Coriolis parameter, and η_x' and η_y' are the zonal and meridional SHA gradients, respectively. The linear trend of EKE for the same period shows extreme values of −230 and 291 cm^2/s^2 per decade (Figure 10b). These EKE trends over the region of study are significant to the 70% level. This lower significance is consistent with the inherently noisy character of the EKE compared with SHA. The region between 30°S and 40°S in the southern portion of the subtropical gyre exhibits the largest trends of EKE, which are indicative of a change in upper ocean dynamic conditions.

[22] These linear trends in SHA and EKE indicate that the changes in the gyre are not spatially uniform. The trends in SHA indicate that, for example, the Zapiola gyre increased its surface height, while the positive trends in EKE on the edges of the anticyclone suggest a strengthening of its anticyclonic circulation. The largest trends in SHA found in the zonal region between 32°S and 35°S are indicative of a deepening of the isotherms in the southern region of the subtropical gyre, together with an increase of EKE in the same region. In addition, there is a change in dynamic height that is concurrent with an alternation of positive and negative EKE trends, south and north of the Confluence region, indicating that the main circulation in this area of the gyre has shifted to the south.

[23] The trend of SST is determined for the same period using fields from the NOAA Optimal Interpolation SST analyses [*Reynolds and Smith*, 1994]. Unlike the trends of SHA, which are positive almost everywhere, the SST trends show a large-scale pattern of positive and negative values in the region of the subtropical gyre. In the subtropical gyre and Confluence region, the trends of SST exhibit extreme

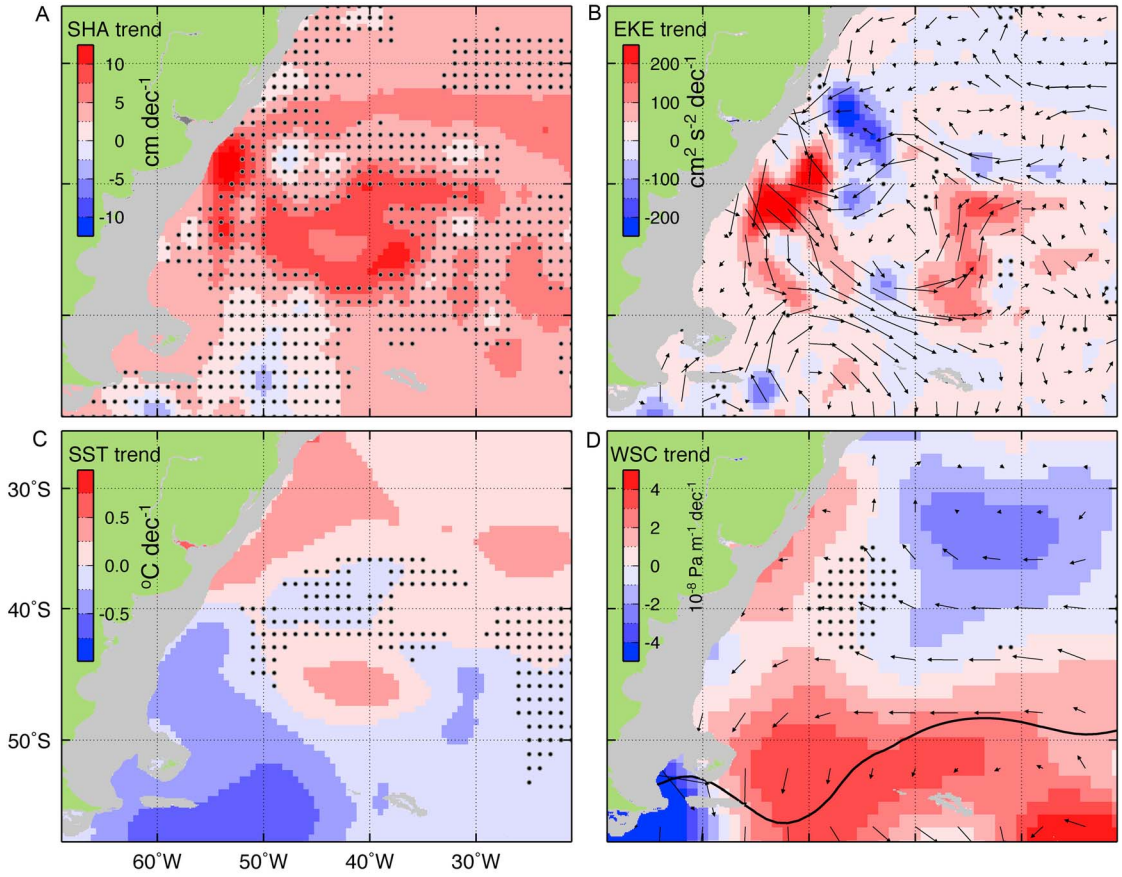

Figure 10. Linear trend of the interannual variability of (a) altimetry-derived sea height anomaly (SHA), (b) altimetry-derived eddy kinetic energy (EKE) and surface geostrophic currents (arrows), (c) sea surface temperature (SST), and (d) wind stress curl (WSC) and wind stress (arrows), during 1993–2006. Stippling indicates linear trends that are not statistically significant to 95% for SHA and 67% for SST, EKE and WSC. The solid black line in Figure 10d indicates the climatological zero-curl contour for the period 1993–2006.

values of −0.83 and 0.89°C per decade (Figure 10c) with a clear basin-wide spatial pattern, where positive trends are located in the interior of the gyre, the Zapiola anticyclone, and Benguela Current regions. SST trends are significant to the 60% level, consistent with the noisier nature of the SST fields compared with SHA. In the subtropics, the variability of the sea height is approximately proportional to the variability of the depth of the isotherms within the main thermocline waters and to the upper ocean heat storage below the mixed layer [e.g., *Mayer et al.*, 2001]. Therefore, the increase in SHA is equivalent to an increase in upper ocean heat storage below the mixed layer. Trends in SST may also be indicative of a change in upper ocean heat storage in the mixed layer of the subtropical gyre. Therefore, these results are consistent with a warming of the water column between the sea surface and the main thermocline.

[24] Trends of wind stress (Figure 10d, arrows) and WSC (Figure 10d, colors) are used to explore possible links between these two parameters and the observed variability in the BCF. These trends are significant to the 60% level. The trends of wind stress are very small in most of the area occupied by the subtropical gyre, except for the band south of the gyre between 32°S and 50°S, where easterly trends (i.e., weakened westerlies) are verified with extreme values of −0.020 and −0.014 Pa per decade. This area of negative τ^x trends is located east of the Confluence region in the region of largest changes in SHA. The negative trend in the wind stress field at approximately 30°S implies slower westerly winds over the southern boundary of the subtropical gyre, possibly increasing the heat storage of the upper ocean by reducing latent and sensible heat fluxes. The spatial pattern of the WSC trend (Figure 10d), with a positive (negative) anomaly south (north) with respect to the climatological zero-curl line, indicates a southward shift of this line, which drives a southward shift of the confluence region. Clearly, the mechanisms invoked to explain the annual-mean location of the separation of the BC can partly explain the long term trends of the separation of the BCF from the continental shelf break.

4. Conclusions

[25] A 15-yearlong record of satellite observations of sea height and sea surface temperature is used to assess the low frequency variability and year-to-year trends of the Brazil Current front during 1993–2008. Given the record length, it cannot be determined whether these trends may be associated with long-period changes or with secular trends.

Results indicate that the separation of the BC shifted southward by approximately 1.5 degrees in latitude during the 1993–2008 period. This change of more than 100 km represents an important departure from the mean location of the frontal region compared, for instance, with the seasonal cycle that exhibits changes of approximately 400 km. This shift cannot be explained by changes in the relative transport between the BC and MC, as proposed by theory and simple models. Using wavelet analysis we show that the periodicity of the separation of the BCF from the continental shelf break changed from an semiannual and annual to a biannual periodicity during 2003. The analysis of trajectories of surface drifter observations cannot be used to conclusively support these results due to the low number of drifter observations. However, trajectories of synthetic drifters generated using altimetry-derived geostrophic currents indicate that there is a shift of the BCF to the south. The positive trends found south of the line of zero WSC agrees with the findings that the BCF is shifting to the south. Positive trends in the SST in the region of the subtropical gyre and the BCF, together with positive trends in the SHA, suggest an increase in the upper ocean heat content. As records of satellite observations become longer, the nature of these signals will be more clearly understood. Ultimately, the attribution of these changes can only be attempted through comprehensive numerical experiments using state-of-the-art ocean models. Attribution of the low frequency variability of the BC front will ultimately contribute to improved understanding of the upper ocean circulation in the South Atlantic and its link with climatic signals and the global ocean circulation.

[26] **Acknowledgments.** The altimeter products were produced by Ssalto/Duacs and distributed by AVISO, with support from CNES. Microwave OI SST data are produced by Remote Sensing Systems and sponsored by the National Oceanographic Partnership Program (NOPP), the NASA Earth Science Physical Oceanography Program, and the NASA REASoN DISCOVER Project. Data are available at www.remss.com. One degree resolution SST data are from NOAA Optimal Interpolation SST analyses. NCEP Reanalysis data are provided by the NOAA/OAR/ESRL PSD from their web site at http://www.cdc.noaa.gov/. Quality controlled drifter data are from the NOAA/AOML Drifter Assembly Center (http://www.aoml.noaa.gov/phod/dac/gdp.html). The authors thank Shenfu Dong for providing constructive comments. This work is supported by the NOAA Climate Program Office.

References

Cabanes, C., A. Cazenave, and C. Le Provost (2001), Sea level change from Topex-Poseidon altimetry for 1993–1999 and possible warming of the Southern Oceans, *Geophys. Res. Lett.*, *28*(1), 9–12, doi:10.1029/2000GL011962.

Conkright, M. E., et al. (1998), World ocean database 1998 CD-ROM data set documentation, Version 2.0, *NODC Internal Rep. 14*, 116 pp.

Ducet, N., P.-Y. Le Traon, and G. Reverding (2000), Global high-resolution mapping of ocean circulation from TOPEX/Poseidon and ERS-1 and −2, *J. Geophys. Res.*, *105*(C8), 19,477–19,498, doi:10.1029/2000JC900063.

Fetter, A., and R. Matano (2010), The remotely and locally wind-forced variability of the South Atlantic Ocean, *Deep Sea Res.*

Garzoli, S. L. (1993), Geostrophic velocity and transport variability in the Brazil-Malvinas confluence, *Deep Sea Res.*, *40*, 1379–1403, doi:10.1016/0967-0637(93)90118-M.

Goni, G. J., and I. Wainer (2001), Investigation of the Brazil Current front variability from altimeter data, *J. Geophys. Res.*, *106*, 31,117–31,128, doi:10.1029/2000JC000396.

Gordon, A. L., and C. L. Greengrove (1986), Geostrophic circulation of the Brazil-Falkland Confluence, *Deep Sea Res., Part A*, *33*, 573–585, doi:10.1016/0198-0149(86)90054-3.

Greenslade, D. J. M., D. B. Chelton, and M. G. Schlax (1997), The mid-latitude resolution capability of sea level fields constructed from single and multiple satellite altimeter datasets, *J. Atmos. Oceanic Technol.*, *14*, 849–870, doi:10.1175/1520-0426(1997)014<0849:TMRCOS>2.0.CO;2.

Grinsted, A., J. C. Moore, and S. Jevrejeva (2004), Application of the cross wavelet transform and wavelet coherence to geophysical time series, *Nonlinear Process. Geophys.*, *11*, 561–566, doi:10.5194/npg-11-561-2004.

Kalnay, E., et al. (1996), The NCEP/NCAR 40-year reanalysis project, *Bull. Am. Meteorol. Soc.*, *77*, 437–470, doi:10.1175/1520-0477(1996)077<0437:TNYRP>2.0.CO;2.

Le Traon, P.-Y., and G. Dibarboure (1999), Mesoscale mapping capabilities of multiplesatellite altimeter missions, *J. Atmos. Oceanic Technol.*, *16*, 1208–1223, doi:10.1175/1520-0426(1999)016<1208:MMCOMS>2.0.CO;2.

Le Traon, P.-Y., and F. Ogor (1998), ERS-1/2 orbit improvement using TOPEX/POSEIDON: The 2 cm challenge, *J. Geophys. Res.*, *103*, 8045–8057, doi:10.1029/97JC01917.

Le Traon, P.-Y., P. Gaspar, F. Bouyssel, and H. Makhmara (1995), Using TOPEX/Poseidon data to enhance ERS-1 data, *J. Atmos. Oceanic Technol.*, *12*, 161–170, doi:10.1175/1520-0426(1995)012<0161:UTDTED>2.0.CO;2.

Le Traon, P.-Y., F. Nadal, and N. Ducet (1998), An improved mapping method of multisatellite altimeter data, *J. Atmos. Oceanic Technol.*, *15*, 522–534, doi:10.1175/1520-0426(1998)015<0522:AIMMOM>2.0.CO;2.

Lentini, C., G. Goni, and D. Olson (2006), Investigation of Brazil Current rings in the confluence region, *J. Geophys. Res.*, *111*, C06013, doi:10.1029/2005JC002988.

Lumpkin, R., and S. L. Garzoli (2011), Interannual to decadal variability in the southwestern Atlantic's surface circulation, *J. Geophys. Res.*, *116*, C01014, doi:10.1029/2010JC006285.

Matano, R. P. (1993), On the separation of the Brazil Current from the coast, 1993. *J. Phys. Oceanogr.*, *23*, 79–90, doi:10.1175/1520-0485(1993)023<0079:OTSOTB>2.0.CO;2.

Mayer, D., R. Molinari, M. Baringer, and G. Goni (2001), Transition regions and their role in the relationship between sea surface height and subsurface temperature structure in the Atlantic Ocean, *Geophys. Res. Lett.*, *28*, 3943–3946, doi:10.1029/2001GL013331.

Peterson, R. G. (1992), The boundary currents in the western Argentine Basin, *Deep Sea Res.*, *39*, 623–644, doi:10.1016/0198-0149(92)90092-8.

Peterson, R. G., and L. Stramma (1991), Upper-level circulation in the South Atlantic Ocean, *Prog. Oceanogr.*, *26*, 1–73, doi:10.1016/0079-6611(91)90006-8.

Reynolds, R. W., and T. M. Smith (1994), Improved global sea surface temperature analyses, *J. Clim.*, *7*, 929–948, doi:10.1175/1520-0442(1994)007<0929:IGSSTA>2.0.CO;2.

Rio, M.-H., and F. Hernandez (2004), A mean dynamic topography computed over the world ocean from altimetry, in situ measurements, and a geoid model, *J. Geophys. Res.*, *109*, C12032, doi:10.1029/2003JC002226.

Ryan, E. H., A. J. Mariano, D. B. Olson, and R. H. Evans (1996), Global sea surface temperature and currents, *Eos Trans. AGU*, *77*(46), Fall Meet. Suppl., Abstract OP22A-16.

Saraceno, M., C. Provost, A. R. Piola, J. Bava, and A. Gagliardini (2004), Brazil Malvinas Frontal System as seen from 9 years of advanced very high resolution radiometer data, *J. Geophys. Res.*, *109*, C05027, doi:10.1029/2003JC002127.

Spadone, A., and C. Provost (2009), Variations in the Malvinas Current volume transport since October 1992, *J. Geophys. Res.*, *114*, C02002, doi:10.1029/2008JC004882.

Veronis, G. (1973), Model of world ocean circulation, I: Wind-driven, two-layer, *J. Mar. Res.*, *31*, 228–288.

Vivier, F., and C. Provost (1999a), Direct velocity measurements in the Malvinas Current, *J. Geophys. Res.*, *104*, 21,083–21,103, doi:10.1029/1999JC900163.

Vivier, F., and C. Provost (1999b), Volume transport of the Malvinas Current: Can the flow be monitored by TOPEX/POSEIDON? *J. Geophys. Res.*, *104*, 21,105–21,122, doi:10.1029/1999JC900056.

Willis, J. K., D. Roemmich, and B. Cornuelle (2004), Interannual variability in upper ocean heat content, temperature, and thermosteric expansion on global scales, *J. Geophys. Res.*, *109*, C12036, doi:10.1029/2003JC002260.

Witter, D., and A. Gordon (1999), Interannual variability of South Atlantic circulation from 4 years of TOPEX/POSEIDON satellite altimeter observations, *J. Geophys. Res.*, *104*(C9), 20,927–20,948, doi:10.1029/1999JC900023.

F. Bringas, P. N. DiNezio, and G. J. Goni, NOAA Atlantic Oceanographic and Meteorological Laboratory, 4301 Rickenbacker Causeway, Miami, FL 33149, USA. (gustavo.goni@noaa.gov)